LTV-MPC for Yaw Rate Control and Side Slip Control with Dynamically Constrained Differential Braking

Article *in* European Journal of Control · December 2009

DOI: 10.3166/ejc.15.468-479

4 authors, including:

Giovanni Palmieri
Università degli Studi del Sannio
26 PUBLICATIONS **307** CITATIONS
SEE PROFILE

Stefano Scala
Stellantis
49 PUBLICATIONS **519** CITATIONS
SEE PROFILE

Luigi Glielmo
Università degli Studi del Sannio
278 PUBLICATIONS **5,200** CITATIONS
SEE PROFILE

European Journal of Control (2009)3-4:468–479

DOI:10.3166/EJC.15.468–479

European Journal of Control

LTV-MPC for Yaw Rate Control and Side Slip Control with Dynamically Constrained Differential Braking

Osvaldo Barbarisi[1,*], Giovanni Palmieri[1,**], Stefano Scala[2,***] and Luigi Glielmo[1,****]

[1]Dipartimento di Ingegneria, Università del Sannio, Plaza di Roma, 21, 82100 Benevento, Italy;
[2]ELASIS S.C.p.A, Via Ex Aeroporto, 80038 Pomigliano D'Arco (NA), Italy

In this paper a novel vehicle lateral dynamic control approach is presented. A differential braking control law based on vehicle planar motion has been designed using a two-degrees-of-freedom vehicle model. On the basis of the estimate of tire longitudinal forces we estimate the range of lateral forces which the tire can exert. Using this constraints a model predictive control (MPC) based on a two-track model is designed in order to stabilize the vehicle. The performances are estimated comparing the results with standard manoeuvers. Simulation results show the benefits of the control methodology used: in particular we show how very effective distribution of braking torque are obtained as a result of this feedback policy.

Keywords: Vehicle Dynamics Control, Model Predictive Control

1. Introduction

Vehicle Dynamic Control (VDC) systems that prevent vehicles from spin and drift out using differential braking have been developed by many manufacturers and proven to significantly improve vehicle lateral stability and safety [21]. These systems, indeed, are used to achieve improved vehicle performance and stability, rendering the vehicle more enjoyable and more comfortable to drive [6, 14].

The VDC is designed to detect a difference between the vehicle response requested by the driver through his/her control input and the actual response of the vehicle. When differences are detected, the system intervenes to correct the path of the vehicle. This automatic reaction is engineered for improved vehicle stability, particularly during severe cornering and on low-friction road surfaces, by helping to reduce over-steering and under-steering.

Many vehicle systems, including stability control and lateral position control, require measurements or estimation of yaw rate and vehicle side slip angle for enhancing stability performance. In such cases, the control system attempts to ensure that the actual yaw rate of the vehicle tracks a desired yaw rate determined by the driver's steering input [19]. However, in situations of low-friction road surfaces, it is also beneficial to control the vehicle side slip angle preventing it from becoming too large [13, 19]. Side slip angle control is necessary because high value of side slip angle can reduce the ability of the tires to generate lateral forces and can significantly compromise the performance of the vehicle control system. Hence, both yaw rate and vehicle side slip angle are variables needed for vehicle stability control.

The control inputs available to control the lateral dynamics can be divided into three groups: the front (and sometimes rear) steering angle, the braking force

**Correspondence to:* G. Palmieri, E-mail: palmieri@unisannio.it
*E-mail: barbarisi@unisannio.it
***E-mail: glielmo@unisannio.it
****E-mail: stefano.scala@elasis.it

Received 2 November 2008; Accepted 11 May 2009
Recommended by A. Edelmayer

(differential braking) and the engine torque, which is usually utilized in conjunction with the other two.

Active steering is more widely used for unmanned control of a vehicle because most drivers would feel uncomfortable without a direct mechanical link between the steering wheel and the tires [3, 4]. Differential braking is the method usually employed in vehicle stability control systems [1, 2, 7, 18, 19] and employs a suitable split of the braking forces among the tires. Other controllers integrate the differential braking technique with the use of the engine torque so that it is possible to achieve the stability goal without slowing down the longitudinal response of vehicle. There are different configurations of these controller types depending on the possibility offered by the driveline of distributing the engine torque among the wheels, e.g active differential on the front wheels only or on all wheels [8, 16, 18, 23].

In this paper we focus our attention on the differential braking approach. We use a standard hierarchical control scheme [8, 22], shown in Fig. 1 and described in details in Section 3; our main contribution consists of replacing a set of decoupled SISO controllers with a model based MIMO controller following the ideas of [9], i.e. a Linear Time Varying (LTV) Model Predictive Control (MPC). We differ from [9] in that the reference signal, rather than being pre-computed, is computed online on the basis of the current value of the steering wheel angle and longitudinal velocity of vehicle and with the use of the bicycle model of the vehicle. The goal of the control is to limit the variations of yaw rate and vehicle side slip angle with respect to the same signals obtained by a two-track model of the vehicle. The control strategy evaluates the set of feasible control inputs depending on the actual states of each wheel. However estimation of forces for each tire of the vehicle is necessary.

Early studies on linear parameter varying (LPV) MPC schemes can be found in [5, 12]. In general, the performance of such a scheme is highly dependent on the nonlinearities of the model since, as the state and input trajectories deviate from the current operating point, the model mismatch increases. However the effectiveness of the proposed MPC formulation was demonstrated on an autonomous vehicle with pre-computed trajectories in [4, 9]; in these papers the authors show simulation and experimental results on an icy surface with 21 ms sample time.

The performance of our work is weighed by using the FMVSS No. 126 standard introduced by the National Highway Traffic Safety Administration (NHTSA) of the United States Department of Transportation [10].

This paper is structured as follows. Section 2 describes the vehicle dynamic model; Section 3 describes in details the functionalities of each control strategy component; in Section 4 we present the simulation results obtained with three kinds of commercial vehicles (class B, class E and class F); in Section 5, the principal aspects of work and the future activities are summarized.

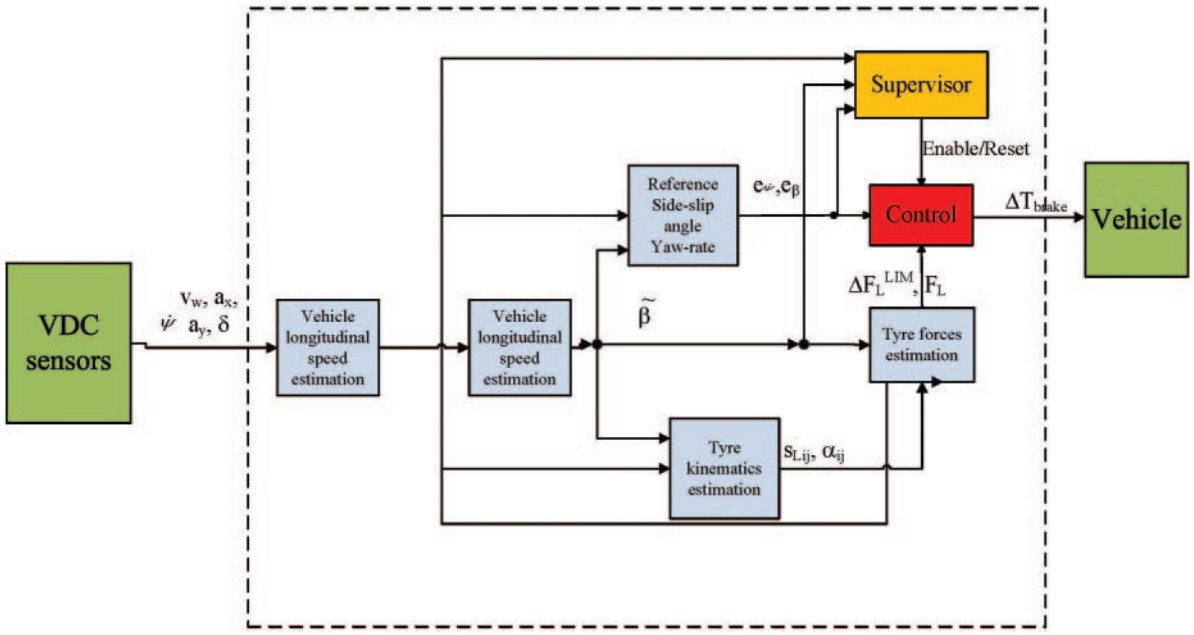

Fig. 1. Dynamic vehicle control strategy.

Nomenclature

$(\cdot)_{ij}$ the subscript i stands for F (front) or R (rear), the subscript j stands for L (left) or R (right), with respect to the body axis system depicted in Fig. 1
α_{ij} wheel side slip angle
β vehicle side slip angle
$\widetilde{\beta}$ estimated β
δ wheel turn angle
μ_{ij} tire-road friction coefficient
ω_{ij} angular speed of the tire
$\dot{\psi}$ yaw rate
$e_{\dot{\psi}}$ error between yaw rate and yaw rete reference
$e_{\tilde{\beta}}$ error between estimated vehicle side slip angle and vehicle side slip angle reference
$\dot{\psi}_{ref}$ reference yaw rate
a_x vehicle longitudinal acceleration
a_y vehicle lateral acceleration
c_{ij} tire cornering stiffness
h distance from center of gravity (CoG) to the road
l_a longitudinal distance from CoG to the front axle
l_b longitudinal distance from CoG to the rear axle
$2l_c$ track width
M mass of the vehicle
r_{ij} rolling radius of the tire
s_{ij} longitudinal slip ratio
v vehicle velocity
v_{ch} characteristic speed
v_{Lij} longitudinal velocity of the tire center
v_x velocity of the vehicle along the x direction
v_y velocity of the vehicle along the y direction
F_{Lij} longitudinal force on the tire
F_{Sij} lateral force on the tire
F_{Zij} vertical force on the tire
J_z yaw inertia moment of vehicle around the z-axis
J_w inertia of wheel around the y-axis
T_s sampling time
T_B braking torque

2. Lateral Vehicle Dynamics Model

The double track model of the vehicle is depicted in Fig. 1; the dynamics of the vehicle are described in details in [2, 13] and reported in equations (1) for the sake of completeness. There M is the vehicle mass; J_z is the vehicle moment of inertia about yaw axis:

$$\begin{bmatrix} \dot{\beta} \\ \ddot{\psi} \end{bmatrix} = \begin{bmatrix} f_1\left(v, \beta, \dot{\psi}, \delta, F_{L_{ij}}, F_{S_{ij}}\right) \\ f_2\left(v, \beta, \dot{\psi}, \delta, F_{L_{ij}}, F_{S_{ij}}\right) \end{bmatrix}, \tag{1a}$$

$$\begin{aligned} f_1\left(v, \beta, \dot{\psi}, \delta, F_{L_{ij}}\right) = \frac{1}{Mv}\{&(F_{L_{FL}} + F_{L_{FR}})\sin(\beta + \delta) \\ &- (F_{S_{FL}} + F_{S_{FR}})\cos(\beta - \delta) \\ &+ (F_{L_{RL}} + F_{L_{RR}})\sin\beta - (F_{S_{FR}} + F_{S_{RR}})\cos\beta\} - \dot{\psi}, \end{aligned} \tag{1b}$$

$$\ddot{\psi} = \frac{1}{J_z}\begin{Bmatrix} \cos\delta(F_{S_{FR}} + F_{S_{FL}})\cdot l_a + \sin\delta(F_{L_{FR}} + F_{L_{FL}})\cdot l_a \\ -(F_{S_{RL}} + F_{S_{RR}})\cdot l_b \\ +\cos\delta(F_{S_{FR}} - F_{S_{FL}})\cdot l_c - \sin\delta(F_{L_{FR}} - F_{L_{FL}})\cdot l_c \\ +(F_{S_{RR}} - F_{S_{RL}})\cdot l_c \end{Bmatrix} \tag{1c}$$

The state-space vector is made of the side slip angle of vehicle β and the yaw rate $\dot{\psi}$. (In the following we will often omit the indices i, j to indicate specific wheel quantities when this does not cause confusion and simplifies notation.) The inputs are given by the wheel turn angle δ.

(1) Lateral and longitudinal forces: The interaction forces between the wheel and the ground are described by Pacejka's formulas which we simplify by assuming that, for each wheel, the longitudinal force (resp., the lateral force) depends only on the longitudinal slip (resp., only on the side slip angle), i.e. [17]:

$$f_L(s; \mu, F_z) = \tilde{f}_L(s; \mu, \alpha, F_z)|_{\alpha=0}, \tag{2a}$$

$$f_S(\alpha; \mu, F_z) = \tilde{f}_S(\alpha; \mu, s, F_z)|_{s=0}, \tag{2b}$$

where $\tilde{f}_L$ and $\tilde{f}_S$ are the full (i.e., combined) Pacejka's formulas for longitudinal and lateral force, α is the wheel side slip angle, that is the angle between the longitudinal wheel axle and the velocity vector $\mathbf{v}$. In the following we will often omit the dependence on μ and F_z for the sake of simplicity. The functions f_L (pure longitudinal, i.e. driving/braking) and f_S (pure lateral, i.e. cornering) are odd w.r.t. s and α respectively.

Finally the tire stiffness coefficients are defined as [13].

$$c(\alpha; \mu, F_z) := \frac{\partial f_S(\alpha; \mu, F_z)}{\partial \alpha} \tag{3}$$

3. Vehicle Dynamic Control Strategy

The algorithm we propose here assumes the following variables to be directly measured: δ, $\dot{\psi}, \omega_{ij}, a_y$ and a_x; while the variables β and v have to be estimated on the basis of the above-mentioned measurements. A control strategy scheme is depicted in Fig. 1. Given the vehicle velocity v, a proper safety bound for the side slip angle β is computed; on the basis of v and the steering wheel angle δ we compute a reference yaw rate signal $\dot{\psi}_{\text{ref}}$ (i.e., the yaw rate "desired" by the driver). When either the difference between the actual yaw rate and the reference yaw rate exceeds a safety range or the vehicle side slip angle exceeds the bound, the Supervisor block enables the Control block which

computes the braking torques to be applied independently to each wheel. While $\dot{\psi}$ is measured, β needs to be estimated.

3.1. Vehicle Side Slip Angle Estimation

The side slip angle estimate $\tilde{\beta}$ is given by [13, 19]

$$\dot{\tilde{\beta}} = -\frac{\dot{v}}{v_x}\sin\tilde{\beta} + \frac{a_y}{v_x} - \dot{\psi}, \tag{4}$$

where in turn v and v_x are estimated according to [11]. By practical experience we noticed that (4) has a problem of error propagation, and thus, a dynamical reset $k_{\text{reset}} \in \{0, 1\}$ has been introduced:

$$\dot{\tilde{\beta}} = -\frac{\dot{v}}{v_x}\sin\tilde{\beta} + \frac{a_y}{v_x} - \dot{\psi} - k_{\text{reset}}\tilde{\beta}. \tag{5}$$

The reset k_{reset} is enabled ($k_{\text{reset}} = 1$) when:

(1) the steering wheel is in neutral position: $|\delta| < \Delta_\delta$;
(2) the vehicle is not rotating: $|\dot{\psi}| < \Delta_{\dot{\psi}}$;
(3) the estimated value of β is not equal to zero $|\tilde{\beta}| > \Delta_\beta$;
(4) conditions (1), (2), (3), are true for a certain period of time T_{On};

where $\Delta_\delta, \Delta_{\dot{\psi}}$ and Δ_β are suitable thresholds.

3.2. Requirements on $\dot{\psi}$ and $\tilde{\beta}$

(1) Reference yaw rate: To compute this we first remind the relation between a given steering angle the corresponding yaw rate at steady state for a bicycle model, given by [19, p. 231]

$$\dot{\psi}_{\text{Ack}} := \frac{v_x}{l\left(1 + v_x^2/v_{ch}^2\right)}\delta, \tag{6}$$

where $l = l_a + l_b$. (The bicycle model is intrinsically stable w.r.t. the velocity v_x for understeering cars, i.e. such that $c_F l_a < c_R l_b$; for oversteering cars, i.e. such that $c_F l_a > c_R l_b$, the bicycle model is asymptotically stable provided v_x is less than the characteristic speed v_{ch} [19].) Then, we compute a bound to take into account the physical limitation of the vehicle: in particular, neglecting $\dot{\beta}$ and $\dot{v}$ in (11), it is possible compute a bound as

$$\dot{\psi}_{\max} = \frac{a_{y_{\max}}}{v_x}, \tag{7}$$

where $a_{y_{\max}}$ is the nominal maximum lateral acceleration. Now, we define $\dot{\psi}_b$ as

$$\dot{\psi}_b = \dot{\psi}_{\max}\text{sat}\left(\frac{\dot{\psi}_{\text{Ack}}}{\dot{\psi}_{\max}}\right) \tag{8}$$

where "sat" denotes the saturation function. The signal $\dot{\psi}_b$ is then smoothed by a unit gain low pass filter whose poles are obtained by the linearization around $\tilde{\beta} = 0$ and $\dot{\psi} = 0$ of (1):

$$W(p) := \frac{a}{p^2 + bp + a}, \tag{9}$$

with

$$a(v) = \frac{c_F c_R l^2 + mv^2(c_R l_b - c_F l_a)}{J_z mv},$$
$$b(v) = \frac{\left(J_z + ml_a^2\right)c_F + \left(J_z + ml_b^2\right)c_R}{J_z mv}.$$

Hence, the reference signal of the yaw rate is given by

$$\dot{\psi}_{\text{ref}} := W(p)\dot{\psi}_b \tag{10}$$

and *we can define* the yaw rate error as $e_{\dot{\psi}} := \dot{\psi} - \dot{\psi}_{\text{ref}}$.
(2) Bounds on the vehicle side slip angle: Following [13, p. 322] we require $\tilde{\beta}$ to be limited in the interval $[-\beta_{\max}, \beta_{\max}]$ where

$$\beta_{\max} := \begin{cases} 2\dfrac{k_1 - k_2}{v_{ch}^3}v^3 - 3\dfrac{k_1 - k_2}{v_{ch}^2}v^2 + k_1 & \text{if } v < v_{ch}, \\ k_2 & \text{if } v \geq v_{ch} \end{cases}. \tag{11}$$

The above formula gives a smoothed version of the plot of reference, as showed in Fig. 2 (notice the deadzone when $\tilde{\beta}$ lies within the bound); reasonable values for parameters k_1 and k_2 are $k_1 = 10°\pi/180°$ and $k_2 = 3°\pi/180°$. Let us define the error variable:

$$e_{\tilde{\beta}} := \begin{cases} \tilde{\beta} + \beta_{\max} & \text{when } \tilde{\beta} < -\beta_{\max}, \\ 0 & \text{when } \tilde{\beta}(t) \in [-\beta_{\max}, \beta_{\max}], \\ \tilde{\beta} - \beta_{\max} & \text{when } \tilde{\beta} > \beta_{\max}. \end{cases} \tag{12}$$

3.3. Tire Kinematics Estimation

(1) Tire side slip angle: The tire side slip angle α is the angle between the wheel velocity vector v and the longitudinal axis of the wheel itself (see Fig. 3). It results:

$$\alpha_{\text{FL}} = -\delta + \text{atan}\left(\frac{v\sin\tilde{\beta} + l_a\dot{\psi}}{v\cos\tilde{\beta} - l_c\dot{\psi}}\right) \simeq -\delta + \tilde{\beta} + \frac{l_a\dot{\psi}}{v}, \tag{13a}$$

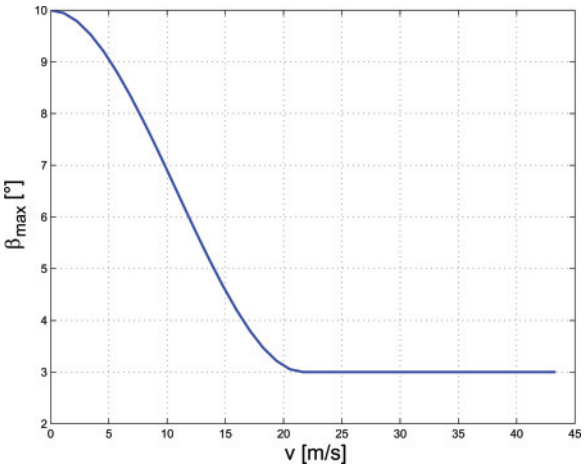

Fig. 2. Dependence of maximum vehicle body side slip angle on speed.

$$\alpha_{\mathrm{FL}} = -\delta + \operatorname{atan}\left(\frac{v\sin\tilde{\beta} + l_a\dot{\psi}}{v\cos\tilde{\beta} + l_c\dot{\psi}}\right) \simeq -\delta + \tilde{\beta} + \frac{l_a\dot{\psi}}{v}, \tag{13b}$$

$$\alpha_{\mathrm{RL}} = \operatorname{atan}\left(\frac{v\sin\tilde{\beta} - l_b\dot{\psi}}{v\cos\tilde{\beta} - l_c\dot{\psi}}\right) \simeq \tilde{\beta} - \frac{l_b\dot{\psi}}{v}, \tag{13c}$$

$$\alpha_{\mathrm{RR}} = \operatorname{atan}\left(\frac{v\sin\tilde{\beta} - l_b\dot{\psi}}{v\cos\tilde{\beta} + l_c\dot{\psi}}\right) \simeq \tilde{\beta} - \frac{l_b\dot{\psi}}{v}, \tag{13d}$$

where we suppose $\cos\tilde{\beta} \simeq 1, \sin(\tilde{\beta}) \simeq \tilde{\beta}$ and $v \gg |l_c\dot{\psi}|$.
(2) Longitudinal slip ratio: The longitudinal slip ratio is defined as [17]

$$s := \frac{r\omega - v_L}{\max\{r\omega; v_L\}}, \tag{14}$$

where r is the actual rolling radius of the tire, ω is the angular speed of the tire (which is measured) and v_L is the linear speed of the tire center along the longitudinal axis of the wheel (which is estimated, e.g. $v_{L_{RR}} = v_x + l_c\dot{\psi}$).

3.4. Vertical Tire Forces Computation

Assuming pitch and roll motions are negligible, single vertical forces on each tire can be estimated separately. Indeed by neglecting suspensions dynamics of the vehicle, the four forces of contact to road of the tires coincide with the vertical forces F_z. By balancing the torques at the points of contact between tires and the surface road, one gets [13, p. 306]

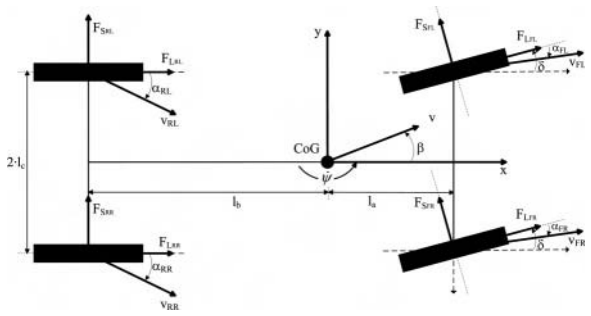

Fig. 3. Double track vehicle model.

$$F_{z_{FL}} \cong \frac{1}{2}\frac{l_b}{l_a+l_b}mg - \frac{1}{2}\frac{h}{l_a+l_b}ma_x + \frac{l_b}{l_a+l_b}\frac{h}{l_c}ma_y, \tag{15a}$$

$$F_{z_{FR}} \cong \frac{1}{2}\frac{l_b}{l_a+l_b}mg - \frac{1}{2}\frac{h}{l_a+l_b}ma_x - \frac{l_b}{l_a+l_b}\frac{h}{l_c}ma_y, \tag{15b}$$

$$F_{z_{RL}} \cong \frac{1}{2}\frac{l_a}{l_a+l_b}mg + \frac{1}{2}\frac{h}{l_a+l_b}ma_x + \frac{l_a}{l_a+l_b}\frac{h}{l_c}ma_y, \tag{15c}$$

$$F_{z_{RR}} \cong \frac{1}{2}\frac{l_a}{l_a+l_b}mg + \frac{1}{2}\frac{h}{l_a+l_b}ma_x - \frac{l_a}{l_a+l_b}\frac{h}{l_c}ma_y. \tag{15d}$$

3.5. Estimation of Tire Forces

One the slips s and α and the vertical tire forces are estimated, we use the simplified Paceijka's formulas (2) to compute the tire forces F_L and F_S. We assume knowledge of μ.

3.6. Bounds on the Control Inputs

If we represent the longitudinal and lateral forces that the road can exert on the tire as in Fig. 4, they belong to an area depending on conditions of road μ and the vertical forces F_z. We assume (but this can be actually justified on the basis of the combined Pacejka's formulas) that the area can be approximated by the ellipsoid (see Fig. 4)

$$\varepsilon F_L^2 + F_S^2 = r^2, \tag{16}$$

where $r := F_S^{LIM}$ and $\varepsilon := \left(F_S^{LIM}/F_L^{LIM}\right)^2$; F_L^{LIM} and F_S^{LIM} represent the maximum longitudinal force and lateral force respectively, defined as

$$F_L^{LIM}(\mu, F_z) := \max_s f_L(s; \mu, F_z), \tag{17a}$$

$$F_S^{LIM}(\mu, F_z) := \max_\alpha f_S(\alpha; \mu, F_z). \tag{17b}$$

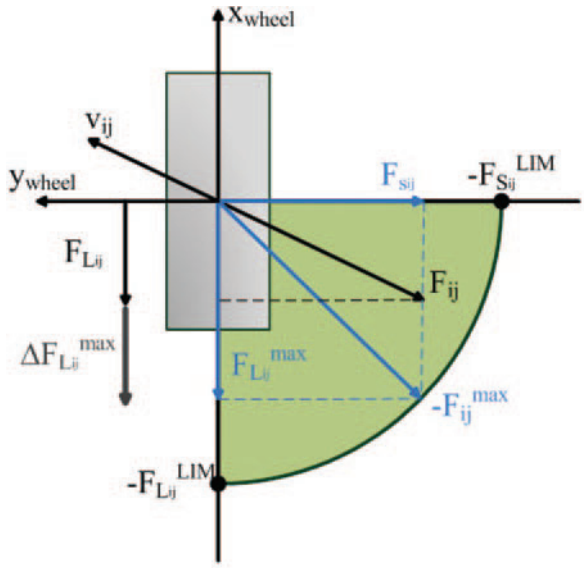

Fig. 4. Lateral and longitudinal forces of the tire inscribed in the ellipsoid of adherence.

Given the actual side force F_S, the allowed longitudinal force that avoids the unstable slipping of the wheel is given by

$$F_L^{\max} := \sqrt{\frac{1}{\varepsilon}\left[r^2 - (F_S)^2\right]}. \tag{18}$$

Finally we point out that, since we are considering the braking action of the tires, rather than the acceleration action, the longitudinal forces F_L will be negative (see Fig. 4) and the "maximum" braking forces corresponding to a side forces F_S will be $-F_L^{\max}$.

3.7. Supervisor

The controller of lateral dynamics is activated when either the error on yaw rate $e_{\dot\psi}$ or the error on side slip angle $e_{\tilde\beta}$ exceed certain respective activations thresholds. The controller is deactivated when both $e_{\dot\psi}$ and $e_{\tilde\beta}$ are within those thresholds for a period T_{rel}. Fig. 5 illustrates the statechart of the corresponding automa.

The thresholds on yaw rate error depends on the vehicle speed. Since the vehicle responds to the steering wheel angle in different manners as the vehicle speed changes, we chose to shape the yaw rate error activation threshold $e_{\dot\psi}^{\text{on}}$ and the deactivation threshold $e_{\dot\psi}^{\text{off}}$ as the following

$$e_{\dot\psi}^{\text{on}}(v_x) = \frac{2v_x/v_{ch}}{\left(1 + v_x^2/v_{ch}^2\right)} e_{\dot\psi}^{\text{ON}} \tag{19a}$$

$$e_{\dot\psi}^{\text{off}}(v_x) = \xi e_{\dot\psi}^{\text{on}}(v_x) \tag{19b}$$

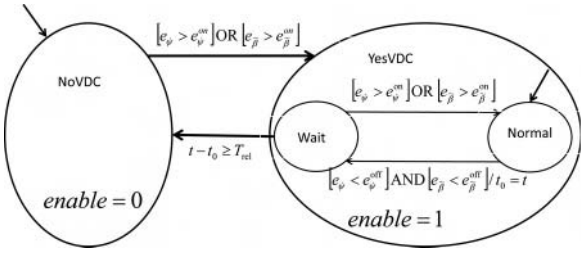

Fig. 5. Statechart of Supervisor. The default state is NoVDC where the boolean signal enable is set to low and the controller is disabled. When one of the two errors signals is outside its threshold, state YesVDC is activated (the boolean signal enable becomes high). The state YesVDC has two child-states: Normal and Wait. The first is the default state, while Wait is activated when both errors are inside the thresholds; if this condition holds for a time $t - t_0 > T_{\text{rel}}$ then the NoVDC is activated.

where $e_{\dot\psi}^{\text{ON}} > 0$ and $\xi \in (0, 1)$, usually $\xi = 0.75$. The reader can see that (19a) is (6) for $\delta = 1$ and divided by $v_{ch}/(2l)$ (which is the maximum yaw rate for $\delta = 1$ attained at $v_x = v_{ch}$); ξ is a calibration parameter.

The side slip angle error activation threshold $e_{\tilde\beta}^{\text{on}}$ has been chosen constant, since in any condition the side slip angle should be small, the deactivation threshold $e_{\tilde\beta}^{\text{off}} = \xi e_{\tilde\beta}^{\text{on}}$.

The delay T_{rel} on the deactivation was introduced after observing that, without it, when the steering wheel angle changes abruptly direction, the controller is disabled (for a very short time) since also the errors on yaw rate and side slip angle change their signs. The authors chose the value of T_{rel} by considering the so called sinus with dwell [10] (see Fig. 7) manoeuvre when the steering wheel angle is 90 [deg]. The candidate value of T_{rel} is the minimum value for which the controller is not disabled during a change of direction of the steering wheel angle. Fig. 6 shows an example of enabling signal.

3.8. Vehicle Dynamic Controller: Model-Predictive Controller

In this section, we design an MPC controller computing the braking torques at the four wheels, to regulate to zero the error on yaw rate and on side slip angle.

In order to reduce the problem computational complexity, rather than working on the nonlinear model (1), we first compute its linearization around the current state. We remind, in view of (3), $f_S(\alpha + \Delta\alpha) \cong c(\alpha + \Delta\alpha)$. Further, in our control model we consider as input the variation ΔF_L of the tire braking (i.e., negative) forces constrained to

$$-F_L^{\max} \le F_L + \Delta F_L \le 0 \tag{20}$$

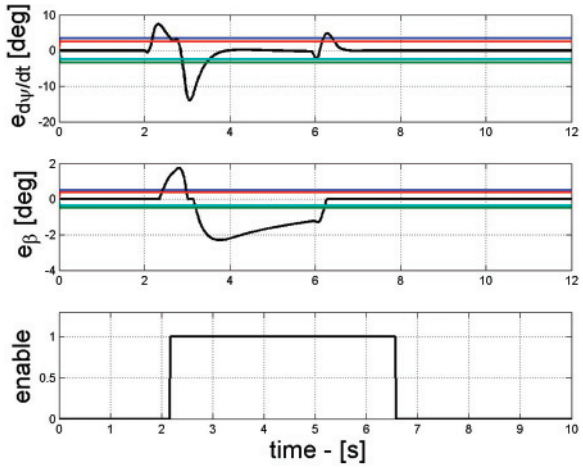

Fig. 6. Example of enabling signal. From the top, side slip angle error $e_{\tilde{\beta}}$ with its thresholds, yaw rate errors $e_{\dot{\psi}}$ with its thresholds and enable signal.

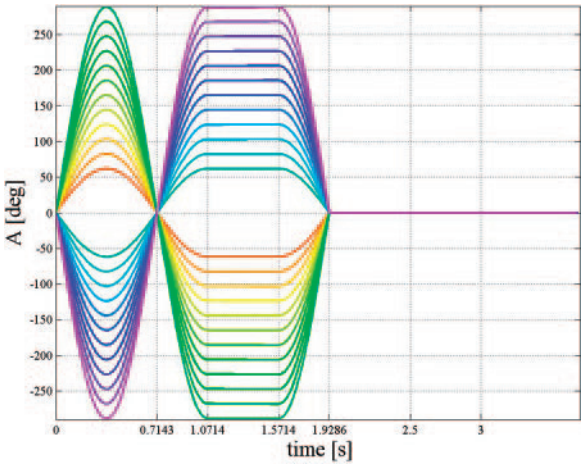

Fig. 7. Sine with Dwell steering profile of various amplitudes.

so that

$$\Delta F_L^{\min} \leq \Delta F_L \leq \Delta F_L^{\max}, \tag{21a}$$

$$\Delta \dot{F}_L^{\min} \leq \Delta \dot{F}_L \leq \Delta \dot{F}_L^{\max}, \tag{21b}$$

where $\Delta F_L^{\min} := -F_L^{\max} - F_L$ and $\Delta F_L^{\max} := -F_L$. Both inequalities represent physical bounds: indeed, (21a) describes the tire forces domain in a particular working point, and the (21b) represents the slew-rate of the braking system. The goal of control is to reduce to zero the errors e_β and $e_{\dot{\psi}}$. The linearized model with e_β and $e_{\dot{\psi}}$ as state variables is

$$\begin{bmatrix} \dot{e}_\beta \\ \dot{e}_{\dot{\psi}} \end{bmatrix} = A\left(\tilde{\beta}, v, \delta, F_L\right) \begin{bmatrix} e_\beta \\ e_{\dot{\psi}} \end{bmatrix} + B\left(\tilde{\beta}, v, \delta\right) \begin{bmatrix} \Delta F_{L_{FL}} \\ \Delta F_{L_{FR}} \\ \Delta F_{L_{RL}} \\ \Delta F_{L_{RR}} \end{bmatrix}, \tag{22}$$

where $A\left(\tilde{\beta}, v, \delta, F_L\right) = \begin{bmatrix} a_{11} & a_{12} \\ a_{21} & a_{22} \end{bmatrix}$ with

$$\begin{aligned} a_{11} &= -\frac{c_F}{mv}(\cos\delta + \delta\sin\delta) - \frac{c_R}{m} - \frac{1}{mv}(F_{L_{FR}} + F_{L_{FL}})\cos\delta + \\ &\quad - \frac{1}{mv}(F_{L_{RR}} + F_{L_{RL}}) - 2\frac{c_F}{mv}\tilde{\beta}\sin\delta - \frac{c_F}{mv^2} l_a \dot{\psi}\sin\delta, \\ a_{12} &= -\frac{l_a c_F}{mv^2}\left(\cos\delta + \tilde{\beta}\sin\tilde{\beta}\right) + \frac{l_b c_R}{mv^2} - 1, \\ a_{21} &= -\frac{l_a c_F}{J_z}\cos\delta + \frac{l_b c_R}{J_z} + (c_{FR}\sin\delta - c_{FL}\sin\delta) l_c, \\ a_{22} &= -\frac{l_a^2 c_F}{J_z v}\cos\delta - \frac{l_b^2 c_R}{J_z v} + (c_{FR}\sin\delta - c_{FL}\sin\delta) l_c; \end{aligned}$$

and where

$$B\left(\tilde{\beta}, v, \delta\right) = \begin{bmatrix} \frac{\sin\delta - \tilde{\beta}\cos\delta}{mv} & \frac{\sin\delta - \tilde{\beta}\cos\delta}{mv} & -\frac{\tilde{\beta}}{mv} & -\frac{\tilde{\beta}}{mv} \\ \frac{l_a \sin\delta - l_c\cos\delta}{J_z} & \frac{l_a \sin\delta + l_c\cos\delta}{J_z} & \frac{l_c}{J_z} & -\frac{l_c}{J_z} \end{bmatrix};$$

finally we define $c_F = c_{FL} + c_{FR}$ and $c_R = c_{RL} + c_{RR}$. The model and its constraints are then time-discretized around the current state $x_k = \left[e_\beta \quad e_{\dot{\psi}}\right]'|_{t=kT_s}$ by using {Euler's method} with sampling time T_s, thus obtaining

$$x_{k+1} = A_T(k)x_k + B_T(k)u_k \tag{23}$$

where $u_k = [\Delta F_{L_{FL}} \quad \Delta F_{L_{FR}} \quad \Delta F_{L_{RL}} \quad \Delta F_{L_{RR}}]'|_{t=kT_s}$ is the control input, $A_T(k) = I + A\left(\tilde{\beta}, v, \delta, F_L\right)|_{t=kT_s} T_s$ is the system matrix, $B_T(k) = B\left(\tilde{\beta}, v, \delta\right)|_{t=kT_s} T_s$ is the input matrix. Let us define $\mathcal{U}_k = [u_k' \quad \ldots \quad u_{k+H_c-1}']'$. By considering a prediction horizon $H_p T_s$, for some interger H_p, in which it is possible to consider with a good approximation:

$$\overline{A}_T = A_T(k) \cong A_T(k+1) \cong \ldots \cong A_T(k+H_p-1), \tag{24a}$$

$$\overline{B}_T = B_T(k) \cong B_T(k+1) \cong \ldots \cong B_T(k+H_p-1), \tag{24b}$$

and by considering a control horizon $H_c T_s$, for some integer $H_c \leqslant H_p$, at each time k we solve the following optimization problem:

$$\mathcal{U}_k^* = \arg\min_{\mathcal{U}_k} \sum_{h=0}^{H_p-1} \left(x_{k+h+1}^c \, Q \, x_{k+h+1} + u_{k+h}^T \, R \, u_{k+h}\right) \tag{25a}$$

subject to

$$x_{k+h+1} = \overline{A}_T x_{k+h} + \overline{B}_T u_{k+h}, \tag{25b}$$

$$x_k = \begin{bmatrix} e_\beta(kT_s) \\ e_{\dot\psi}(kT_s) \end{bmatrix}, \tag{25c}$$

$$u_{k+h+1} = u_{k+h} \quad \forall h \geq H_c - 1, \tag{25d}$$

$$u^{\min} \leq u_{k+h} \leq u^{\max}, \tag{25e}$$

$$\Delta u^{\min} \leq u_{k+h} - u_{k+h-1} \leq \Delta u^{\max}, \tag{25f}$$

where $u_{-1} = 0$. Inequality (25e) is related to (21a) and inequality (25f) is related to (21b).

The cost function (25a) is quadratic and the constraints (25b)–(25f) are linear, therefore the optimization problem (25) is convex and can be solved with efficient quadrating programming (QP) solver (see the Appendix for details).

We denote by $\mathcal{U}_k^* = [u_k^*, \ldots, u_{k+H_c-1}^*]'$ the sequence of optimal braking torques computed at time k by solving problem (25) from the current observed state x_k. Then the first element u_k^* of $\mathcal{U}_k^*$ is actually applied to the system at time k. The algorithm the authors use to transform the forces variation ΔF_L thus obtained into oil pressure variation for the braking system is illustrated in [20].

4. Simulation

To test our control strategy we have chosen a manoeuver known as the 0.7 Hz Sine with Dwell manoeuver. As the name suggests, the manoeuver is a single sinusoidal steering input performed at a frequency of 0.7 Hz, with a 500 ms pause between completion of the third quarter cycle and initiation of the fourth quarter cycle. Fig. 7 shows several such manoeuvers with different amplitudes A.

To begin the manoeuver, the driver accelerates the vehicle to a speed of approximately 52 mph, then the throttle is released and a programmable steering controller is engaged. Once the vehicle has coasted down to a speed of 50 mph, the steering machine automatically executes the steering wheel angle profile.

Since the manoeuver entrance speed is always 50 mph, increasing the amplitude of the steering wheel angles is used to increase manoeuver severity. See (Forkenbrock *et al*. 2004) for details.

We performed the test on three different cars parameterized in Carsim datasets: class B (medium cars), class F (high level cars) and class E (SUV cars).

The tuning parameters, of course, depends on the car. For simplicity we report only the class B tuning:

- the sampling time $T_s = 250$ [ms];
- the H_p horizon: 5;
- the H_c horizon: 3;
- the control weight for side slip angle error $e_{\tilde\beta}$: $q_1 = 1$;
- the control weight for yaw rate error $e_{\dot\psi}$: $q_2 = 10$;
- the control weight matrix R for the variation of longitudinal forces:

$$\text{diag}\left[\frac{10^{-8}|\max_{ij} F_{z_{ij}}|}{|F_{z_{FL}}|}, \frac{10^{-8}|\max_{ij} F_{z_{ij}}|}{|F_{z_{FR}}|}, \frac{10^{-8}|\max_{ij} F_{z_{ij}}|}{|F_{z_{RL}}|}, \frac{10^{-8}|\max_{ij} F_{z_{ij}}|}{|F_{z_{RR}}|}\right];$$

- the deactivation time $T_{\text{rel}} = 0.12$ [s], the side slip error activation threshold $\underset{\sim}{e}{}^{\text{on}}_{\beta} = 0.5$ [deg] and deactivation threshold is $\underset{\sim}{e}{}^{\text{off}}_{\beta} = 0.75\underset{\sim}{e}{}^{\text{on}}_{\beta}$.

The choice of the horizons length is a compromise between computational load and necessary information for the prediction model.

In Fig. 8 the yaw rate behavior is depicted and it is apparent that all (simulated) cars pass the test.

To evaluate the performance we define two indexes of yaw rate according to [10]:

$$J_1 = 100\frac{\dot\psi(t_0 + 1)}{\dot\psi_{\text{peak}}}, \tag{26a}$$

$$J_2 = 100\frac{\dot\psi(t_0 + 1.75)}{\dot\psi_{\text{peak}}} \tag{26b}$$

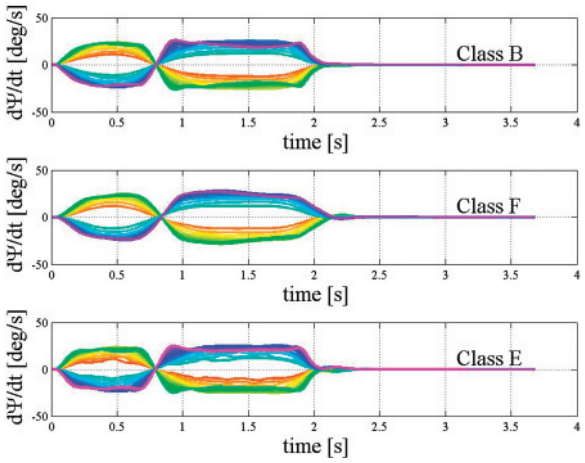

Fig. 8. FMVSS No. 126 test: Yaw rate profiles for various amplitudes of steering manoeuvres. From the top, yaw rate profile of Class B test; yaw rate profile of Class F test; yaw rate profile of Class E test.

where $t_0 = 1.93$ is the instant of steering completion of steer, $\dot{\psi}_{\text{peak}}$ is first yaw rate peak produced after the second steering reversal at 0.71 [s]. In [10] the thresholds $J_1 < 35\%$ and $J_2 < 20\%$ are given. Figs 9 and 10 show the quite promising results of our strategy.

In [10] also an index of the "responsiveness" of the controller is proposed, meaning that the controller, while trying to stabilize the vehicle, should not compromise the lateral displacement imposed by the steering wheel angle. Lateral displacement is defined as the perpendicular distance of the vehicle center of gravity from a line defined by the initial heading (i.e., before the test manoeuver was initiated). Specifically, the index is based on the measure of the lateral displacement at 1.07 seconds, that is the start instant of constant steering angle in the manoeuver. FMVSS No. 126 would require all light vehicles to produce a lateral displacement of at least 6 feet (1.83 m). Fig. 11 shows that our controller satisfies this limit in the simulations with E-Class car, too.

Fig. 12 refers to one manoeuvre of class B about FMVSS No. 126 test with a max amplitude of steering wheel angle of 125° [deg] and suggests some characteristics of the closed loop system. One can notice that the yaw rate tracking is satisfactory and the braking systems utilized the side of vehicle with greater load (and hence with larger adherence ellipse). This is a consequence of:

- the dependence of controller matrix R on the normal forces F_z,
- the time-varying boundaries in the optimal quadratic problem.

Finally the figure shows the variation of longitudinal velocity to verify the assumption of constant value in the prediction interval (250 ms).

The controller here proposed has shown good performances in variety of (simulated) manoeuvres, provided the horizons are not too short and the

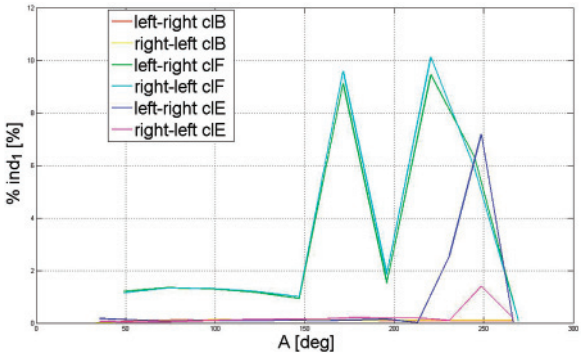

Fig. 9. J_1 index profile against the maximum amplitude (A) of each manoeuvre's steering profile. Left-right: first sine period positive; right-left: first sine period negative.

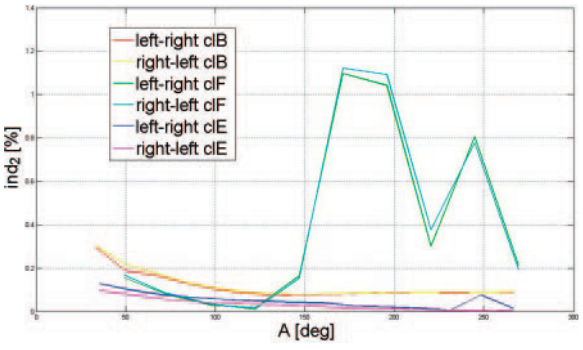

Fig. 10. J_2 index profile against the maximum amplitude (A) of each manoeuvre's steering profile. Left–right: first sine period positive; right-left: first sine period negative.

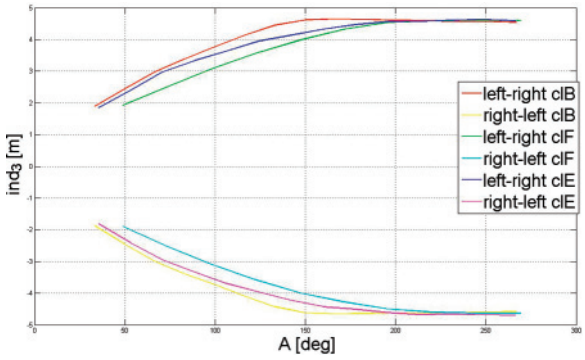

Fig. 11. Lateral displacement profiles: lateral displacement at 1.07 [s] against amplitude A.

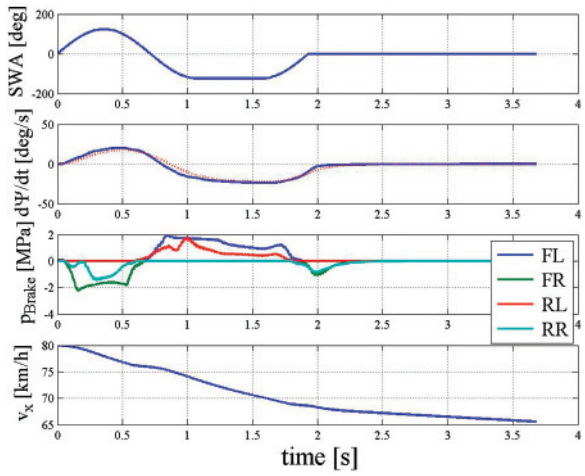

Fig. 12. One manoeuvre of FMVSS No. 126 test. From top, steering angle; yaw rate vs reference yaw rate; wheel braking pressures (for clarity's sake right hand pressures are negative), vehicle longitudinal speed.

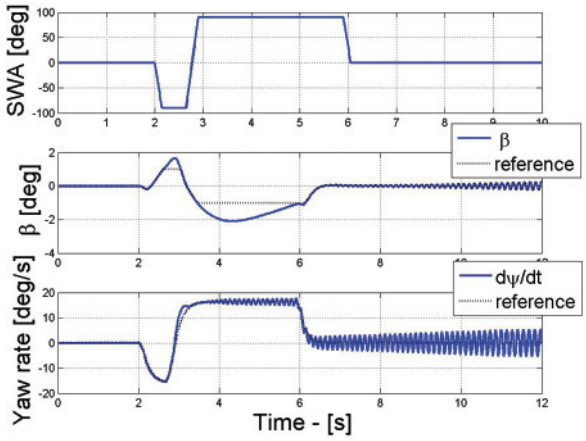

Fig. 13. ATI 90 test @ 90 km/h with bad tuning of controller parameters. From top, steering wheel angle, side slip angle, yaw rate.

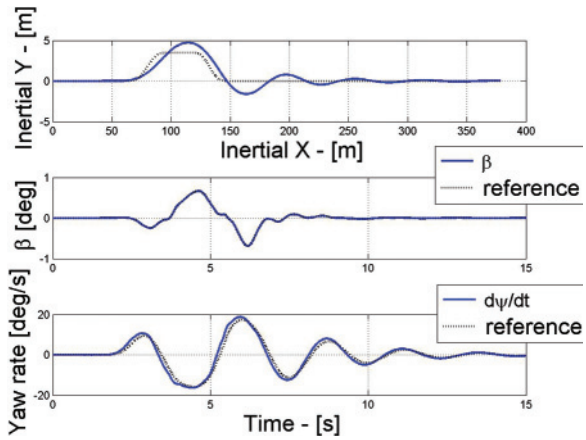

Fig. 14. Double lane change @ 100 km/h. From top, vehicle position in inertial frame vs reference trajectory; side slip angle vs reference side slip angle; yaw rate vs reference yaw rate.

weights on side slip errors and yaw rate errors are not too unbalanced, i.e. $q_2 \cong 10q_1$. Otherwise unstable behavior may occurs as shown in Fig. 13 reporting results of a particular ATI 90 manoeuvre. In this test:

- the value of steering changes from $-90°$ to $90°$,
- the initial speed v is fixed (in our simulation, 90 Km/h),
- the driver releases the accelerator pedal when the manoeuvre starts,
- to "stress" the MPC controller we chose $q_1 = 1$ and $q_2 = 100, H_p = 2, H_c = 1$.

After the third sudden change of the steering wheel angle, the system starts oscillating because the restrictive choice of q_2 forces the controller to work close to constraints boundaries.

5. Conclusions

In this paper, a novel vehicle lateral dynamic control approach has been presented utilizing differential braking. At best of authors' knowledge this is the first published application of LTV MPC technique to design VDC for a non-autonomous vehicle. The simulations were performed on three different Carsim datasets cars that represent different typologies: light cars, oversteering rear traction sport cars, Suv cars. The use of an MIMO controller based on MPC techniques with dynamical constraints yields the desired differential braking.

A future step will be the introduction of engine torque as a further control variable, although with constraints for safety reasons. Another step will be the inclusion of driver in the loop. In our simulated manoeuvres the driver does not interact with the system, and this fundamental assumption has allowed to design the controller considering only the lateral dynamics. If the driver has to track a reference trajectory in global inertial frame, the lateral dynamics controller is not sufficient, as shown in Fig. 14.

The final goal is the experimental test of our strategies on tracks, so as to compare them to the current lateral electronic stability controllers.

Appendix

Formulation of the QP Problems

In this section we present in detail the formulation of the Linear Time Varying (LTV) Model Predictive Control (MPC) problems introduced in Section 3.8 and used for designing braking MPC algorithms.

In the LTV MPC algorithm a discrete-time linear model is used for prediction and optimization. In particular an open loop constrained optimization problem is formulated by using a discrete-time linear prediction model and solved in receding horizon. This prediction model is used in the open loop finite time constrained optimal control problem that is recast as a standard Quadratic Programming (QP) problem. We show how the data matrices of the QP problem are computed from the prediction model.

In Section 3.8 we have formulated the optimization problem in equation (25). To cast it as a QP problem, we first re-write equations (25f) in the form $\tilde{L}V \leq N$, where

$$\tilde{L} = \begin{bmatrix} -L \\ L \end{bmatrix}, \quad L = \begin{bmatrix} I_{4x4} & 0 & \cdots & 0 & 0 \\ -I_{4x4} & I_{4x4} & \ldots & 0 & 0 \\ 0 & -I_{4x4} & \ddots & 0 & 0 \\ \vdots & \vdots & \ddots & \ddots & \vdots \\ 0 & 0 & \ddots & -I_{4x4} & I_{4x4} \end{bmatrix},$$

$$N = \begin{bmatrix} -\Delta u^{\min} - u_{k-1} \\ -\Delta u^{\min} \\ \vdots \\ -\Delta u^{\min} \\ \Delta u^{\max} + u_{k-1} \\ \Delta u^{\max} \\ \vdots \\ \Delta u^{\max} \end{bmatrix}, \quad V = \begin{bmatrix} u_k \\ \vdots \\ u_{k+H_c-1} \end{bmatrix},$$

and $L \in R^{4H_c \times 4H_c}$ and $N \in R^{8H_c}$. Constraints (25e) can straightforwardly be written as $V^{\min} \leq V \leq V^{\max}$, with obvious definitions of matrices $V^{\min}$, $V^{\max}$.

To compute the prediction model, let us define the state prediction vector

$$X = \begin{bmatrix} x_{k+1} \\ x_{k+2} \\ \vdots \\ x_{k+H_p} \end{bmatrix}$$

and construct the control vector $U \in R^{4H_p}$ over the H_p steps of the prediction horizon (out of the shorter vector $V \in R^{4H_c}$ over the control horizon)

$$U = TV, \quad \text{with } T = \begin{bmatrix} I_{4x4} & \cdots & 0 \\ \vdots & \ddots & \vdots \\ 0 & \cdots & I_{4x4} \\ 0 & \ldots & I_{4x4} \\ 0 & \vdots & \vdots \\ 0 & \ldots & I_{4x4} \end{bmatrix}.$$

Now, after introducing the matrices

$$F = \begin{bmatrix} \overline{A}_T \\ \overline{A}_T^2 \\ \vdots \\ \overline{A}_T^{H_p} \end{bmatrix} \quad G = \begin{bmatrix} \overline{B}_T & 0 & \cdots & 0 \\ \overline{A}_T \overline{B}_T & \overline{B}_T & \cdots & 0 \\ \vdots & \vdots & \ddots & \vdots \\ \overline{A}_T^{H_p-1} \overline{B}_T & \overline{A}_T^{H_p-2} \overline{B}_T & \cdots & \overline{B}_T \end{bmatrix}$$

one can compactly re-write equations

$$X = Fx_k + GTV \tag{29}$$

and accordingly re-write in matrix form the cost functional in (25a), so that the whole problem (25) can be formulated as a constrained Quadratic Problem as follows:

$$\mathcal{U}_k^* = \arg\min_V \left[V^T \left(T^T G^T \hat{Q} G T + T^T \hat{R} T \right) V + \right. \\ \left. + 2x_k^T F^T \hat{Q} G T V + x_k^T F^T \hat{Q} F x_k \right], \tag{30a}$$

subject to

$$V^{\min} \leq V \leq V^{\max}, \tag{30b}$$

$$\tilde{L} V \leq N. \tag{30c}$$

Problem (30) is solved by using LSSOL, a software package for solving constrained linear least-squares problems and convex quadratic programs (definite or semi definite) [15].

References

1. Ackermann J. Robust car steering by yaw rate control. In: Proceedings of the 29th IEEE Conference on Decision and Control, vol. 4, pp. 2033–2034
2. Anwar S. Generalized predictive control of yaw dynamics of a hybrid brake-by-wire equipped vehicle. *Mechatronics* 2005; 15: 1089–1108
3. Borrelli F, Bemporad A, Fodor M, Hrovat D. An MPC/hybrid system approach to traction control. *IEEE Trans Control Syst Technol* 2006; 14(3): 541–552
4. Borrelli F, Falcone P, Keviczky T, Asgari J, Hrovat D. MPC based approach to active steering for autonomous vehicle systems. *Int J Veh Auton Syst* 2005; 3(2–3): 265–291
5. Chisci L, Falugi P, Zappa G. Gain-scheduling MPC of nonlinear systems. *Int J Robust Nonlinear Control* 2003; 13: 295–308
6. Chung T, Yi K. Design and evaluation of side slip angle-based vehicle stability control scheme on a virtual test track. *IEEE Trans Control Syst Technol* 2006; 14(2): 224–234
7. Daily R, Bevly DM. The use of GPS for vehicle stability control systems. *IEEE Trans Ind Electron* 2004; 51(2), 270–277
8. Kim D, Kim K, Lee W, Hwang I. Development of Mando ESP (electronic stability program). In: Proceeding of the 2003 SAE World Congress, 2003, number SAE 2003-10-0101
9. Falcone P, Borrelli F, Asgari J, Tseng HE, Hrovat D. Predictive active steering control for autonomous vehicle systems. *IEEE Trans Control Syst Technol* 2007; 15(3): 566–580
10. Forkenbrock G, O'Harra B, Elsasser D. A demonstration of the dynamic tests developed for NHTSA's light vehicle rollover research program – phase viii of NHTSA's light vehicle rollover research program. In: NHTSA Technical Report, 2004.
11. Imslanda L, Johansena TA, Fossena TI, Gripa HF, Kalkkuhlb JC, Suissa A. Vehicle velocity estimation using nonlinear observers. *Automatica* 2006; 42: 2091–2103
12. Keviczky T, Balas GJ. Flight test of a receding horizon controller for autonomous UAV guidance. In: Proceedings of the American Control Conference, 2005.

13. Kienke U, Nielsen L. *Automotive Control Systems*. Springer: Germany, 2000
14. Koleszar P, Trencseni B, Palkovics L. Development of an electronic stability program completed with steering intervention for heavy duty vehicles. In: Proceedings of the IEEE International Symposium on Industrial Electronics, 2005, Vol. 1, pp. 379–384
15. LSSOL-solver (n.d.). www.sbsi-sol-optimize.com
16. Ouladsine M, Shraim H, Fridman L, Noura H. Vehicle parameter estimation and stability enhancement using the principles of sliding mode. In: Proceedings of the American Control Conference ACC '07, 2007, pp. 5224–5229
17. Pacejka H. *Tire and Vehicle Dynamics*. SAE International: UK, 2006
18. Piyabongkarn D, Rajamani R, Grogg JA, Lew JY. Development and experimental evaluation of a slip angle estimator for vehicle stability control, *IEEE Trans on Control Syst Technol* 2009; 17: 78-88
19. Rajamani R. *Vehicle Dynamics and Control*. Springer-Verlag, New York, 2005
20. Solyom S, Rantzer A, Ludemann J. Synthesis of a model-based tire slip controller. *Veh Syst Dyn* 2004; 41(6): 475–499
21. Tseng HE, Ashrafi B, Allen Brown T, Recker D. The development of vehicle stability control at ford. *IEEE/ASME Trans Mechatronics* 1999; 4(3): 223–234
22. van Zanten AT, Erthadt R, Pfaff G. VDC, the vehicle dynamics control of Bosch. In: Proceeding of the International Congress and Exposition, 1995, SAE950759, 1995, pp. 9–26
23. Zhao S, Li Y, Zheng L, Lu S. Vehicle lateral stability control based on sliding mode control. In: Proceedings of the IEEE International Conference on Automation and Logistics, 2007, pp. 638–642